Int. J. Nanosci. Nanotechnol., Vol. 10, No. 2, June 2014, pp. 67-78

Cerium-Promoted PtRu/MWNTs As the Anode Catalyst for Methanol Electro-Oxidation

E. Esmaeili[1,2,3,*], A. M. Rashidi[3], Kh. Jafari-Jozani[3]

1- Birjand University of Technology, Department of Chemical Engineering, Birjand, I. R. Iran.
2- Catalysis and Nanostructured Materials Research Laboratory, School of Chemical Engineering, College of Engineering, University of Tehran, Tehran, I. R. Iran.
3- Research Institute of Petroleum Industry (RIPI), Tehran, I. R. Iran

(*) Corresponding author: e.esmaeily@gmail.com
(Received:19 July 2013 and accepted: 26 Feb. 2014)

Abstract:
In the present study, PtRuCe/MWNTs nanocatalysts synthesized via polyol process technique are applied as anode electro-catalyst in methanol electro-oxidation reaction (MOR). To characterize the nanocatalysts, TEM, XRD, EDS and XPS are investigated. Cyclic voltammetry and choronoamperometry are used to evaluate the electro-catalytic activity and stability of the catalysts in methanol electro-oxidation, respectively. Further addition of the Ce promoter to MWNTs-supported PtRu nanocatalyst shows the highest activity and the lowest onset potential in MOR at Ce to Pt molar ratio of 0.7. A significant enhancement of the forward anodic peak in cyclic voltammetry experiments is observed for the Ce-promoted PtRu catalyst with cerium to platinum molar ratio of 0.7, i.e. 349 mA/cm^2.mg$_{Pt}$, in comparison with 182 mA/cm^2.mg$_{Pt}$ and 251 mA/cm^2.mg$_{Pt}$, respectively, corresponding to Pt/MWNTs and PtRu(1:1)/MWNTs nanocatalysts. Furthermore, the chronoamperommetry results present a remarkable improvement in the final current density of PtRuCe/MWNTs (6.1 mA/cm^2), compared to the un-promoted catalysts, having a decreasing propensity, i.e. PtRu/MWNTs (3.7 mA/cm^2) and Pt/MWNTs (2.05 mA/cm^2.mgcat). The improved performance of PtRuCe/MWNTs may be attributed to the formation of highly-dispersed Pt nanoparticles on the support, followed by a significant enhancement of bi-functional mechanism, as a result of cerium incorporation.
Keywords: *Multi-walled carbon nanotubes, Bi-functional mechanism, Fuel cells, Methanol electro-oxidation.*

1. INTRODUCTION

Fuel cells, especially, direct methanol fuel cells (DMFCs) as energy conversion devices have attracted so much attention in recent decades, because of high efficiency and low emission [1].
Platinum has been recognized as an excellent anode material for DMFCs, in especial, at lower temperatures [2-3]. The formation of CO-like intermediates on Pt active sites upon MOR may lead to the blockage of the active sites, decreasing the overall efficiency. According to literature [3], CO intermediate species formed over Pt active sites could be oxidized via incorporating the second metal such as ruthenium, i.e. bi-functional mechanism. Since, PtRu catalyst is not able to eliminate the CO species, thoroughly; some modifications over a PtRu/MWNTs catalyst are structurally required [3]. It is found that alloying Pt with oxophilic elements is a proper way to improve the catalytic performance of Pt in MOR, activating the water molecules [4]. In

fact, oxophilic nature of metal oxides with several oxidation states could be helpful to remove the strongly adsorbed intermediates, especially, CO, from the platinum active sites via formation of appropriate amounts of OH_{ads} which in turn, lowers the required potential to oxidize CO to CO_2 [5-7]. According to literature [8-9], oxygen vacancies of ceria give a promising chance to gain a high oxygen storage capacity. Furthermore, as reported in the literature [10-11], ceria could enhance the dispersion of metal crystallites and stabilize the support in contrast to thermal sintering. Guo *et al.* [5] developed a carbon-supported PtRu-CeO_2 as anode electrocatalyst for DMFC, considering the large oxygen storage capacity of ceria. Based on what they observed, CeO_2-promoted PtRu catalysts showed the higher electrochemical activities than the un-promoted ones.

They rationalized that the formation of PtRu alloy along with ceria which presents a transition oxidation states ($Ce^{3+}\leftrightarrow Ce^{4+}$) in an amorphous form could be responsible for higher electrochemical performance. Xu *et al.* [12] postulated that OH^- anion adsorption at lower potentials leads to the formation of OH_{ads} species over CeO_2 are highly capable to convert CO-like intermediate species formed on the transition metal to CO_2, making the active sites profitable for further electrochemical reaction. According to what ascribed in the literature [5, 13], OH groups, owing a significant ability to intensify bi-functional mechanism, could enhance through the shift consecutively occurred between the reduced and the oxidized states ($Ce^{3+}\leftrightarrow Ce^{4+}$) of cerium oxide which in turn, facilitates the oxygen mobility in crystal lattice [14].

In the current study, PtRu/MWNTs nanocatalysts promoted by ceria were prepared via polyol process technique to apply as anode electrode catalyst of direct methanol fuel cell.

2. EXPERIMENTAL

2.1. Materials

All the chemicals used in the present study were of analytical grade and applied with no further purification. Multi-walled carbon nanotubes were prepared using chemical vapor deposition (CVD) of methane as the carbon resource over Co-Mo/MgO at 900°C [15]. The resulted carbon nanotubes were purified by several washing steps in aqueous solution of HCl and subsequently, HNO_3 (Merck) to eliminate all the impurities, followed by heating at 260°C. Afterwards, MWNTs were functionalized using a mixture composed of sulfuric acid (Merck) and nitric acid with a volumetric ratio of 3:1, respectively, under sonication at 60°C for 3h.

2.1. Preparation method

In the current study, all of the catalysts were synthesized by polyol process technique in which ethylene glycol plays a significant role as reducing agent. Briefly, MWNTs were dispersed in ethylene glycol in an ultrasonic bath for 20 min followed by the addition of desired amounts of metal precursors, i.e. $H_2PtCl_6.6H_2O$ (Aldrich, 40%), $RuCl_3.2H_2O$ (Merck) and $Ce(NO_3).6H_2O$ (Merck) under vigorous stirring. Subsequently, a solution of KOH (Merck) was added to the solution dropwise, adjusting the pH at around 11-12, in order to induce the formation of tiny and uniform catalyst nano particles. The resulting suspension was heated up to ca. 140°C under reflux condition for 3 h, introducing the argon gas into the solution. Afterwards, the product was washed with an abundant amount of deionized water after filtration, followed by drying in vacuum oven at 100°C for 6 h. In this investigation, for all of the catalysts, 20 %wt. of precious metal (i.e. Pt) on MWNTs surface as support was utilized.

2.2. Characterization methods

The morphology of the catalysts was determined by XRD (Philips Diffractometer) equipped with Cu Kα (λ = 1.54056 A°) radiation in 2θ range of 30-90°. The surface morphologies and the cluster diameters were determined by TEM (ZEISS EM 900). EDS (Link Systems AN-10000) analysis was utilized to determine the presence of mineral species in the catalysts. XPS (XR3E2, 8025-BesTec) experiment was applied to investigate the chemical state and the elements existed on the catalyst surface.

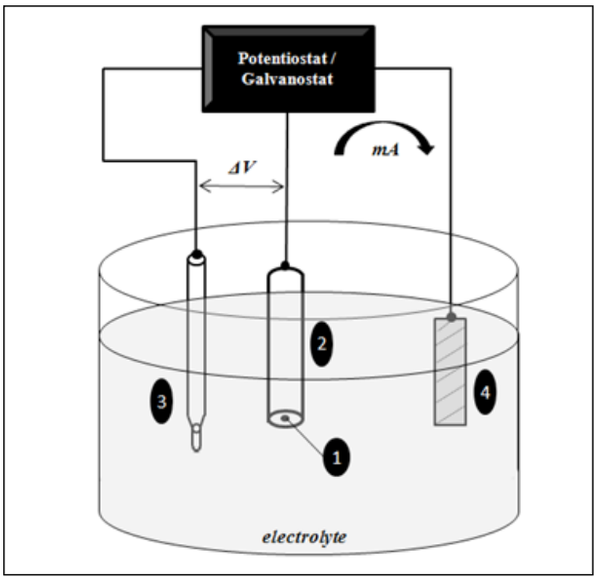

Figure 1: *A schematic representation of the cell used for DMFCs*

1- Modified GC as working electrode
2- Teflon shield of the working electrode
3- Ag/AgCl reference electrode
4- Pt counter electrode

2.3. Preparation of Working Electrodes

Prior to start the electrochemical measurements, we need to prepare the working electrode. The method is to fabricate the glassy carbon (GC) electrode surface using the sonicated homogeneous solution composed of 5 mg catalyst powder dispersed in a mixture of 50µl nafion (Alfa Aesar) in 2 ml ethanol (Merck). The solvent was slowly evaporated using a 100W lamp. Finally, the modified electrode was heated up to 80°C for 30 min in an oven.

2.4. Electrochemical measurements

All the electrochemical experiments were carried out in a conventional three-electrode cell, i.e. working, reference and counter electrodes. In the present study, a Teflon sheathed glassy carbon disk with 2 mm in diameter (0.0314 cm^2) as working electrode, a Pt plate (5.2 cm^2) as counter electrode and an Ag/AgCl electrode as reference one were respectively applied. A schematic presentation of the cell is exhibited in Figure 1. All potentials in this work were considered vs. Ag/AgCl electrode, i.e. 197 mV vs. the standard hydrogen electrode at 25°C. The nitrogen gas was used to purge the electrolyte existed in the cell. To evaluate the electro-oxidation ability of the catalysts, an Ivium Stat electrochemical analyzer (Ivium Technologies, Ivium Stat type 10V/5A) was utilized.

The catalytic assessment of the anode electrode in methanol electro-oxidation reaction (MOR) was determined by cyclic voltammetry (CV) tests in an aqueous solution of 1 M methanol and 0.5 M sulfuric acid. The CV curves were performed at a scan rate of 50 mV/s from -200 mV to 1200 mV (vs. Ag/AgCl), taking into account that a constant value of the current-voltage during the time was

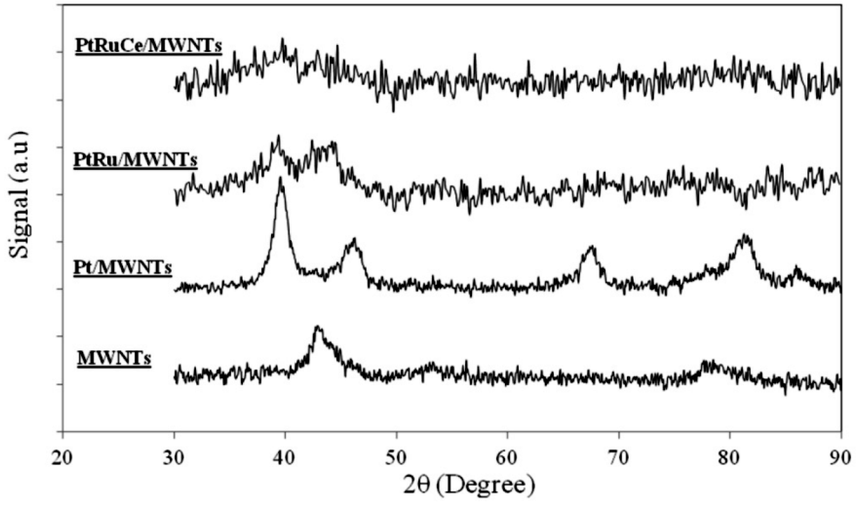

Figure 2: *X-ray diffraction (XRD) patterns of MWNTs, Pt/MWNTs, PtRu/MWNTs, PtRuCe/MWNTs.*

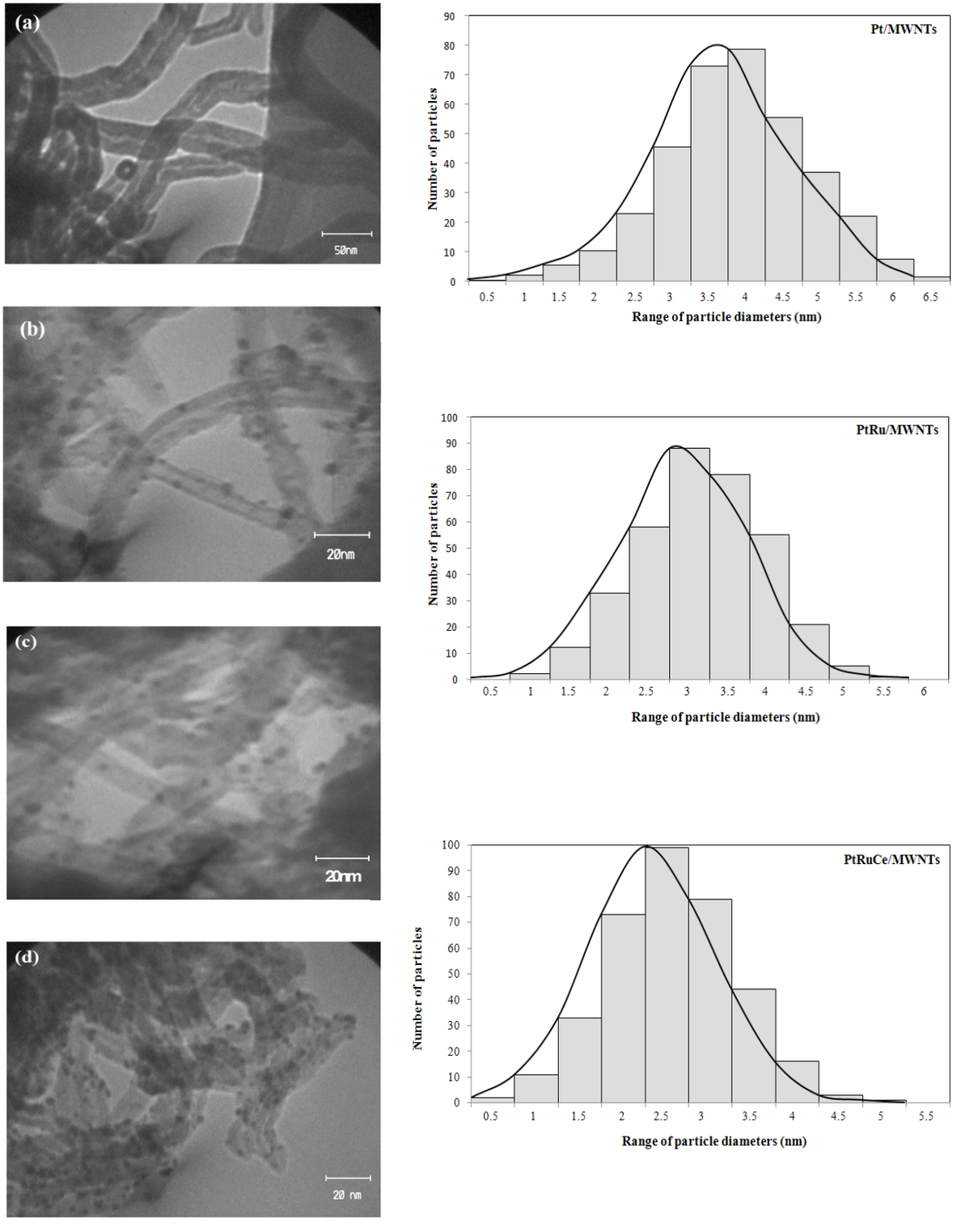

Figure 3: *Transmission electron microscopy of (a) MWNTs, (b) Pt/MWNTs, (c) PtRu/MWNTs, (d) PtRuCe/MWNTs and the corresponding Pt size distributions.*

required. The stability of catalysts was investigated by chronoamperometry analysis at 0.6 V examined for 5400s. Electro-catalytic surface areas (ECSA) were determined by CV experiment in 0.5 M aqueous solution of sulfuric acid at a scan rate of 50 mV/s.

3. RESULTS AND DISCUSSION

The X-ray diffraction (XRD) patterns of MWNTs, Pt/MWNTs, PtRu (1:1)/MWNTs and PtRuCe (1:1:0.7)/MWNTs are shown in Figure 2. The peaks observed for the MWNTs sample at 2θ angles of around 42°, 54°, and 77° are respectively attributed to the planes of (100), (004) and (110) of carbon graphite structure [13]. In the case of Pt/MWNTs, the diffraction peaks appeared at 2θ angles of ca. 40°, 46°, 68°, 81° and 87° are corresponding to (111), (200), (220), (311) and (222) planes of platinum FCC crystallite[16-19]. There is no additional peak in the case of ruthenium- and/or ceria-promoted Pt/MWNTs. This may confirm that ruthenium and cerium oxide species have the amorphous structure and/or very small crystallites in PtRu/MWNTs and PtRuCe/MWNTs. Furthermore, the incorporation of promoters (i.e. Ru or Ce) into Pt/MWNTs leads to no shift in any of the platinum diffraction peaks, indicating that further addition of the promoters examined in the present study doesn't change the crystallographic orientations of platinum catalyst supported on MWNTs [13].

Figure 3 displays the TEM micrographs of MWNTs, Pt/MWNTs, PtRu/MWNTs and PtRuCe/MWNTs. Figure 3a presents a proof regarding to the elimination of the mineral impurities (i.e. Co-Mo species) upon the purification stage, showing an open end of MWNTs. Comparing Figures 3b, c and d reveals the highly well-dispersed Pt nanoparticles, when ruthenium and/or cerium promoters are incorporated into the Pt nanoparticles. The average Pt particle size among ca. 360 randomly selected particles was estimated to be 3.9, 3.1 and 2.6 nm, respectively, corresponding to Pt/MWNTs, PtRu/MWNTs and PtRuCe/MWNTs. Therefore, it seems that the incorporation of Ru and/or cerium into Pt/MWNTs enhances the active surface area of platinum, in accordance with the literature [13].

The energy dispersive X-ray spectroscopy (EDS) of MWNTs-supported Pt, PtRu and PtRuCe samples is shown in Figure 4 to identify the amounts of the elements existed. According to Figure 4, one may conclude that the molar ratio of Pt:Ru in PtRu/MWNTs catalyst is found to be 47.1:52.9, meanwhile, the one of Pt:Ru:Ce in the spectrum belonged to PtRuCe/MWNTs is evaluated to be 35.8:38.2:26.0, in good accordance with the theoretical values applied in the synthesis process. This indicates that the precursors used (i.e. H_2PtCl_6, $RuCl_3$ and $CeNO_3$) might adequately reduce to their corresponding metallic nanoparticles by ethylene glycol through polyol process technique.

XPS spectra of Pt/MWNTs, PtRu/MWNTs, and PtRuCe/MWNTs electrocatalysts are illustrated in Figure 5. According to the figure, the peaks centered at binding energies of ca. 71 eV are associated with

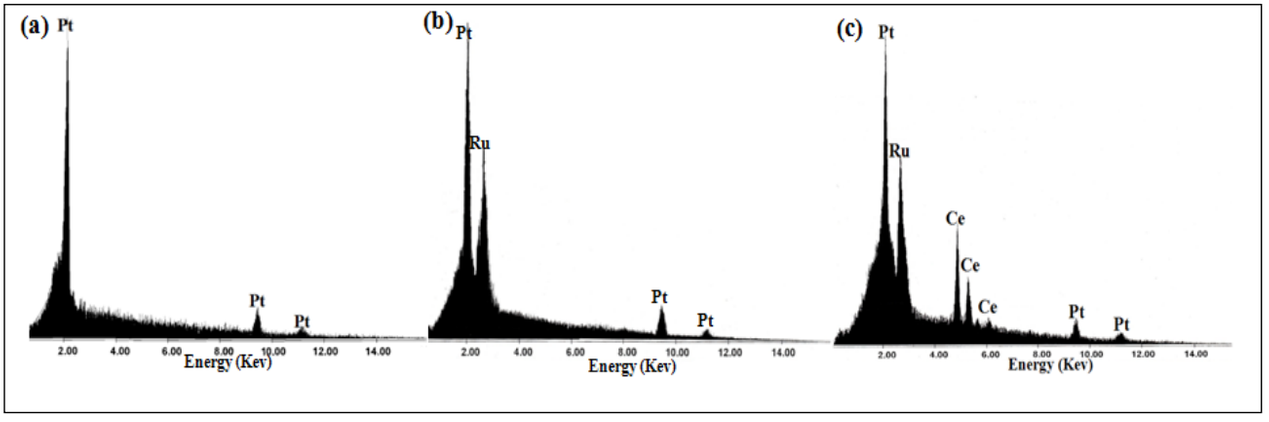

Figure 4: *Energy Dispersive spectra of (a) Pt/MWNTs, (b) PtRu/MWNTs, and (c) PtRuCe/MWNTs.*

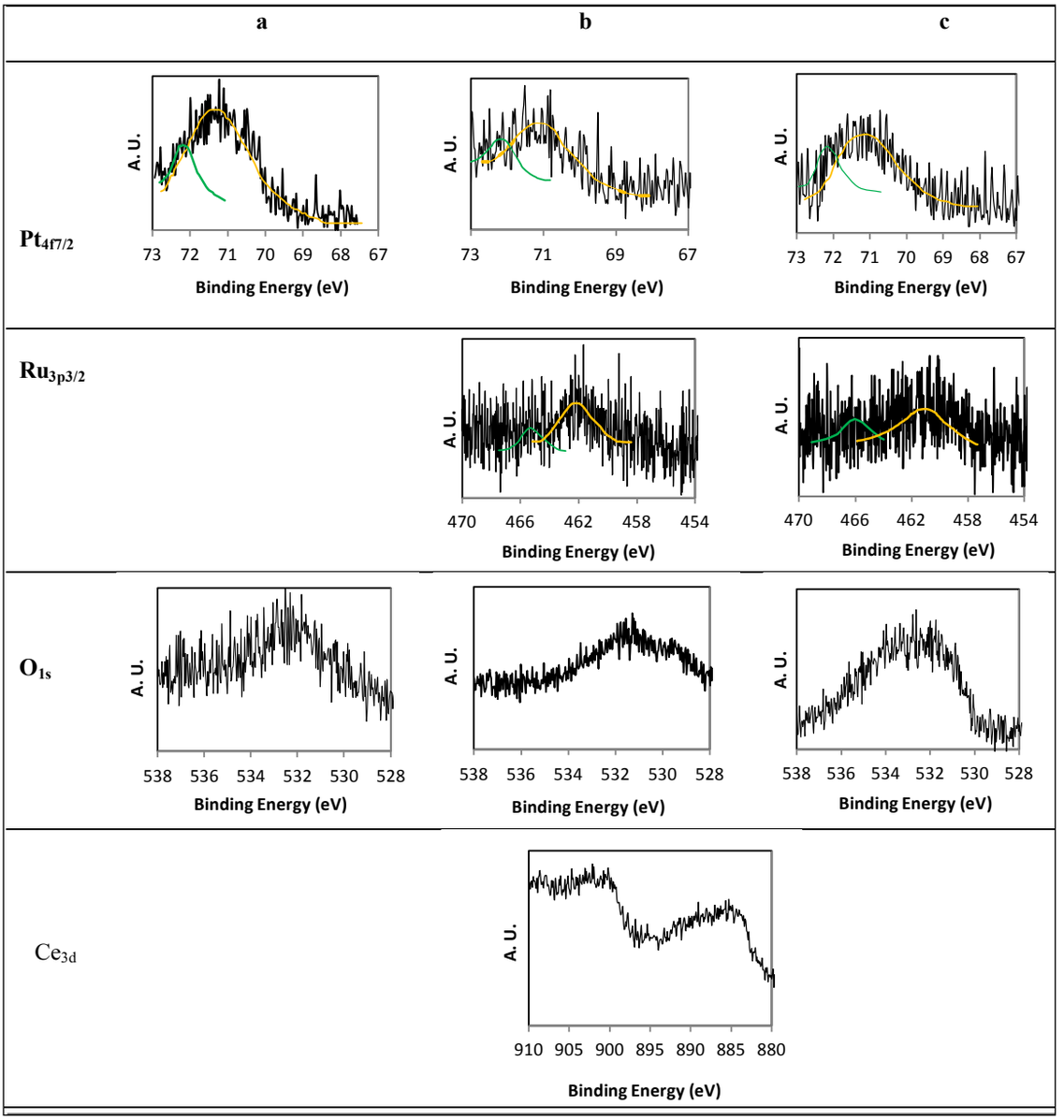

Figure 5: *XPS spectra for $Pt_{4f7/2}$ region, $Ru_{3p3/2}$ and O1s for a) Pt/MWNTs, b) PtRu/MWNTs and PtRuCe/MWNTs*

Pt4f7/2, confirming the presence of zero-valent platinum species, however, the ones at around 72.4 eV may be attributed to the existence of PtO and/ or $Pt(OH)_2$.

As observed in Figure 5, in the case of un-promoted MWNTs-supported Pt catalyst, there is just one peak at binding energy of about 532 eV, followed by a small shoulder, implying the presence of oxygen species located on the carbon surface, i.e. C=O [5], meanwhile, in line with literature [5], two significant O1s oxygen-related peaks in the range of 528–538 eV are expected, assigning to two indicative oxygen-containing chemical species, i.e. those of connected to the carbon nanotube surfaces and the ones associated with the metal oxides.

The peaks centroid at ca. 886.77 and 903.89 eV are also typical of Ce^{3+}, along with the prominent features of Ce^{4+} appeared at 882.74, 889.61 and

Table 1: *The binding energies of $Pt_{4f/2}$ and $Ru_{3p3/2}$, and the relative percentage of surface species of the un-promoted and Ru- and Ce-promoted Pt catalysts.*

Catalyst	Peak	Binding Energy (eV)	Species	At. Percent (%)
Pt/MWNTs	$Pt_{4f7/2}$	71.22	Pt(0)	84
		72.04	Pt(II)	16
PtRu/MWNTs	$Pt_{4f7/2}$	71.0	Pt(0)	77
		72.14	Pt(II)	23
	$Ru_{3p3/2}$	462.1	Ru(0)	73.85
		466.0	Ru(IV)	26.15
PtRuCe/ MWNTs	$Pt_{4f7/2}$	71.05	Pt(0)	71
		72.14	Pt(II)	29
	$Ru_{3p3/2}$	462.05	Ru(0)	72.28
		465.25	Ru(IV)	27.72

901.87 eV, in accordance with literature [13]. Considering the coexistence of two oxidation states of cerium, one may confirm the highly oxygen mobility in the crystal lattice.

Table 1 presents the atomic percents of platinum, ruthenium and cerium based on what observed in Figure 5. According to Table 1, in the case of Pt/MWNTs, the amount of zero-valent Pt is found to be 84%, whereas, the peak associated with the Ru- and Ce-promoted catalysts is less intensified, i.e. 77 and 71%, respectively. Further addition of cerium to PtRu-based catalyst slightly increases the ruthenium atomic percent (at. %) in its (VI) oxidation state from 26.15 to 27.72% at 466.00.04± eV [5]. This may be probably attributed to the preferable reaction of oxygen atoms released from the ceria species with unalloyed metallic Ru nanoparticles in PtRuCe/MWNTs catalyst.

Figure 6 implies the voltammograms of Pt/MWNTs, PtRu/MWNTs and PtRuCe/MWNTs, when the experiment is carried out in desired aqueous solution of 0.5 M H_2SO_4 at room temperature. According to Figure 6, two anodic peaks partially overlapping in the range of -200 mV to 150 mV are observed, indicating desorption of the hydrogen monolayer from platinum active sites. Meanwhile, the cathodic peaks appeared in the same range in the reverse scans may be assigned to the adsorption of atomic hydrogen on the Pt clean surface [3, 20-22]. Moreover, the weakly broad anodic peaks revealed in the range of 200 to 550 mV may be attributed to the hydrogen spillovers from platinum surface towards the supports [5]. As observed in Figure 6, the hydrogen spillover from platinum active sites to the support is facilitated in the following order; PtRuCe/MWNTs > PtRu/MWNTs > Pt/MWNTs. This could guaranty the effective interaction between platinum nanoparticles and the promoters used, i.e. Ru and Ce, which in turn, improves the oxidation-related kinetics on free platinum active sites.

The electrochemical active surface area (ECSA) could be evaluated from Eq. (1), as follows [4]:

$$\mathbf{ESA\ (cm^2/mg_{Pt}.)= 4.76\ QH\ /\ [Pt]} \qquad \mathbf{(1)}$$

where [Pt] stands for the platinum loading existed on the electrode surface (mg/cm^2) and QH (mC/cm^2) is defined as the charge associated with the integrated intensity of the atomic hydrogen desorption peaks [23-24].

From Eq. (1), the electrochemical active surface areas are found to be 13.9, 18.3 and 24.1 m^2/g, in accordance with Pt/MWNTs, PtRu/MWNTs, and PtRuCe/MWNTs, respectively. An indicative enhancement in the active surface area in the presence of ruthenium and cerium is observed,

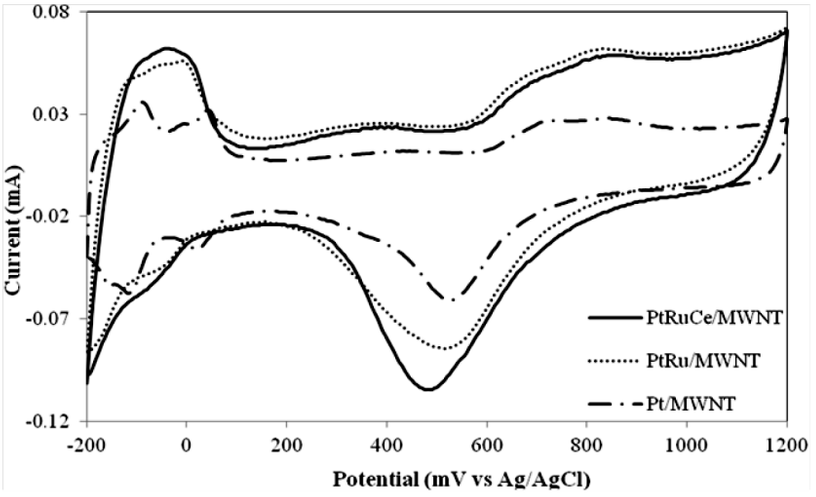

Figure 6: *Cyclic voltammograms of Pt/MWNTs, PtRu/MWNTs, and PtRuCe/MWNTs at scan rate of 50 mV/s in 0.5 M H_2SO_4 at room temperature*

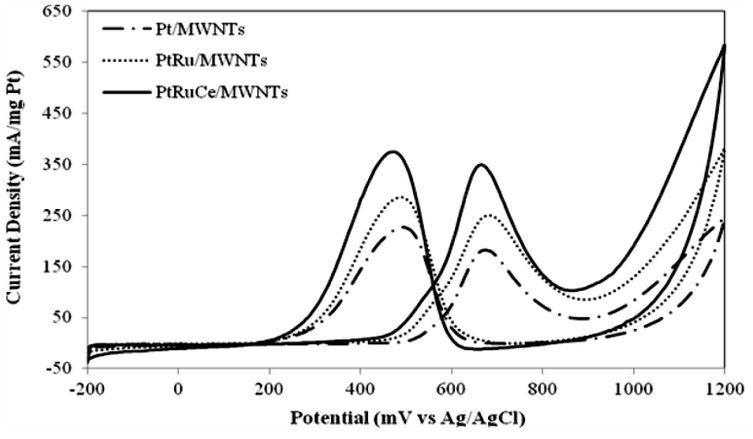

Figure 7: *Cyclic voltammograms for Pt/MWNTs, PtRu/MWNTs, and PtRuCe/MWNTs at scan rate of 50mV/s in aqueous solution of 0.5 M H_2SO_4 and 1 M methanol at room temperature*

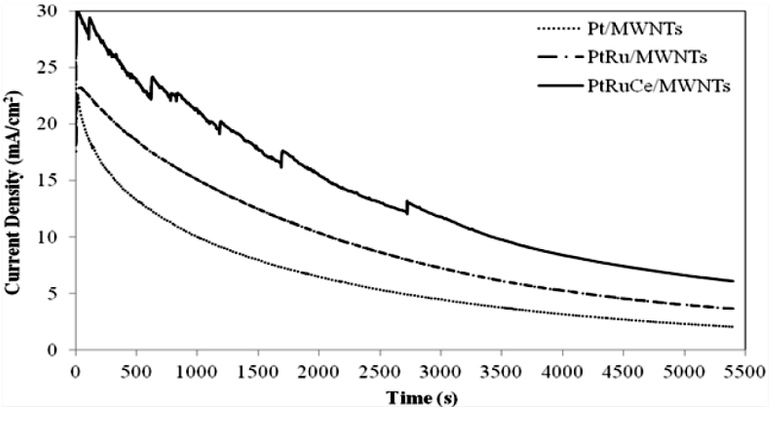

Figure 8: *The results of chronoamperometry experiment of Pt/MWNTs, PtRu/MWNTs and PtRuCe/MWNTs at 0.6 V in aqueous solution of 0.5 M H_2SO_4 and 1 M methanol at room temperature.*

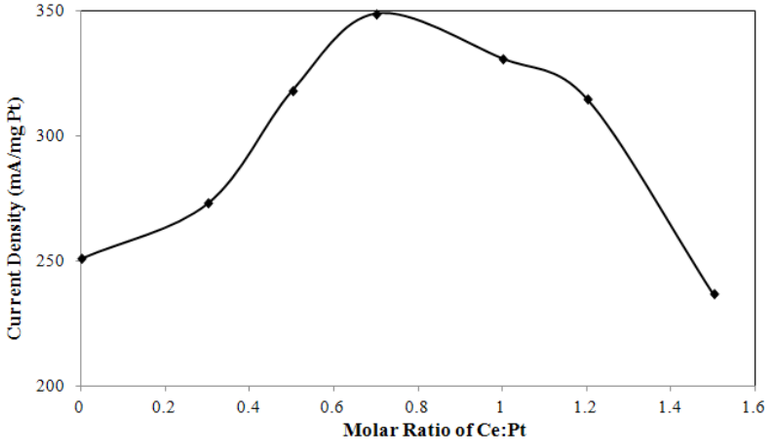

Figure 9: *The variation of the forward peak current density (I_f) of cyclic voltammograms at different molar ratios of cerium to platinum.*

supported by TEM photographs, showing the smaller nanoparticles sizes compared to those of Pt-based sample. Moreover, considering the shift between two different states of cerium oxide, the increase of Pt nanoparticles utilization is expected. This mechanism is illustrated in equations 2 and 3, as supported by Scibioh *et al.* [13]:

$$2Ce^{3+} + Pt^{2+} \longrightarrow 2Ce^{4+} + Pt^{0} \quad (2)$$

and /or

$$4\ Ce^{3+} + Pt^{4+} \longrightarrow 4\ Ce^{4+} + Pt^{0} \quad (3)$$

The results of cyclic voltammetry in an aqueous solution of 0.5 M H_2SO_4 and 1 M methanol are shown in Figure 7. According to Figure 7, the peak current density in the forward scans varies from 182 mA/mg Pt associated with Pt/MWNTs to 251 and 349 mA/mg Pt, respectively, corresponding to PtRu/MWNTs and PtRuCe/MWNTs. Furthermore, the onset potential of methanol electro-oxidation reaction on PtRu/MWNTs and PtRuCe/MWNTs are found to be 461 and 434 mV, respectively, i.e. 31 and 58 mV lower than that of the Pt/MWNTs (492 mV). This confirms the enhancement of platinum catalytic activity in methanol electro-oxidation with further incorporation of cerium and ruthenium.

According to literature [25-26], the ratio of the forward anodic peak current density (I_f) to the reverse one (I_b) may describe the catalyst tolerance in contrast to the accumulation of CO-like species over the catalyst surface. Considering Figure 7, the ratio of the forward peak current density to the backward one shows an increasing propensity with further addition of the promoters used in the current study (i.e. Ru and Ce), as the values of 0.80, 0.87 and 0.93 for the Pt/MWNTs, PtRu/MWNTs and PtRuCe/MWNTs catalysts are obtained. Following the findings described here, the effective removal of the intermediates formed upon the methanol electro-oxidation reaction from the platinum active surfaces in presence of Ce and Ru species is expected.

The chronoamperometry results of un-promoted and promoted Pt catalysts investigated in the present study are depicted in Figure 8. According to Figure 8, the current densities show a continuous decrease upon the experiments for promoted and un-promoted Pt catalysts. As well-known from literature [1-4], due to the adsorption of the poisonous oxygen-containing intermediates of methanol electro-oxidation reaction, a decreasing propensity is expected. However, the final current densities after 5400s increase from 2.04 mA/cm^2 for the un-promoted Pt/MWCNTs to the values of 3.67 and 6.10 mA/cm^2 for PtRu/MWNTs and PtRuCe/MWNTs, respectively. This indicates a significant stability against the poisonous species of the promoted Pt catalysts, in good accordance with the lower onset potentials and the higher ratios of (I_f/I_b) in cyclic voltammograms presented in Figure 7.

In line with the literature [12, 23], the higher activity and stability of PtRu/MWNTs in methanol electro-oxidation compared to those of Pt/MWNTs may be attributed to the synergetic effects of ruthenium via enhancing the bi-functional mechanism.

In order to investigate the effect of ceriumin on the electro-catalytic activity of PtRuCe/MWNTs, different ratios of Ce:Pt was considered. Cyclic voltammetric experiments were performed at room temperature, applying the scan rate of 50 mV/s. In this sense, the molar ratio of Pt:Ru was remained constant at 1:1, meanwhile, the molar ratio of Ce to Pt was changed in the range of 0-1.5. Figure 9 demonstrates the peak current densities in the forward scans (I_f) vs. the amount of molar ratio of Ce:Pt. According to Figure 9, one may observe a distinct maximum If value at Ce:Pt=0.7. Therefore, one may conclude that the spillovers of the poisonous species of adsorbed CO-containing intermediates from platinum sites to the support is more pronounced at cerium to platinum molar ratio of 0.7, in comparison with the other catalysts examined.

To understand the mechanism occurred on the catalyst surface, we need to mention what the intermediates originated from. As we know, platinum active sites play a positive role as the main substrate for dehydrogenation of methanol. Therefore, according to the mechanism presented in the following (Eq. 4), the adsorption of CO-like species connected to the platinum sites is expected. On the other hands, ruthenium sites could effectively dissociate the water molecules, forming OH_{ads} groups located on Ru species (Eq. 5). The OH_{ads} groups interact with the adsorbed CO-containing intermediates presented on platinum surface, releasing the active sites for further methanol oxidation (Eq. 6) [17, 27]. The mechanism is mentioned below.

$$CH_3OH + Pt^0 \longrightarrow Pt - CO_{ads} + 4H^+ + 4e^- \quad (4)$$

$$Ru^0 + H_2O \longrightarrow Ru - OH_{ads} + H^+ + e^- \quad (5)$$

$$PtCO + Ru\text{-}OH_{ads} \longrightarrow Pt^0 + Ru^0 + CO_2 + H^+ + e^- \quad (6)$$

Where Pt^0 and Ru^0 is denoted the zero-valent platinum and ruthenium sites.

Since, the CO groups adsorbed on the ruthenium surface blocks the Ru active sites [28], the formation of $-OH_{ads}$ species on cerium oxide surface may significantly enhance the electro-catalytic activity and stability of PtRuCe/MWNTs compared to those of PtRu/MWNTs through improving the bi-functional mechanism. In fact, as explained previously, the transition metal oxides like ceria, due to their oxophilic nature, are able to dissociate the water, adsorbing the OH groups, which in turn, help the elimination of CO intermediates from the platinum surface through bi-functional mechanism [13].

Furthermore, cerium may change the electron structure of the Pt-based catalyst examined, facilitating the electron transfer towards the platinum [29]. This may facilitate CO oxidation and decrease the CO coverage on platinum surface.

According to above-mentioned results, one may propose that ceria plays a considerable role supported by bi-functional mechanism based on which CO-like intermediates is oxidized through the surface oxygen utilization of cerium oxide [13] (Eq. 7).

$$Pt\text{-}CeO_x + y\ CO \longrightarrow Pt\text{-}CeO_{x-y} + y\ CO_2 \quad (7)$$

4. CONCLUSIONS

Ru- and RuCe-promoted Pt/MWNTs electro-catalysts were synthesized through polyol method to apply in methanol electro-oxidation reaction. MWNTs-supported highly-dispersed Pt nanoparticles with a narrow size distribution was observed, supported by TEM, for Ru- and more considerably, in the case of Ce-incorporated catalysts.

Electrochemical experiments indicated the enhanced performance for the Ce-promoted PtRu/MWCNTs catalysts in the course of activity and stability, especially, at Ce to Pt molar ratio of 0.7. The improvement may be attributed to the intensified bi-functional mechanism strengthened via synergetic effect of cerium and ruthenium, increasing the hydrogen spillover from platinum active sites. Furthermore, surface oxygen of cerium oxide nanoparticles may help to increase Pt active

sites through both oxidation of CO to CO_2 and also, a considerable enhancement of Pt surface area, as a conclusion of higher dispersion.

REFERENCES

1. A. Nouralishahi, A.A. Khodadadi, A.M. Rashidi, Y. Mortazavi, J. Colloid Interface Sci., Vol. 393, No. 1, (2013), pp. 291-299.
2. K. Kakinuma, Y. Chino, Y. Senoo, M. Uchida, T. Kamino, H. Uchida, Sh. Deki, M. Watanabe, Electrochim. Acta, Vol. 110, (2013), pp. 316-324.
3. D. Dixon, J. Melke, M. Botros, J. Rathore, H. Ehrenberg, C. Roth, Int. J. Hydrogen Energy, Vol. 38, No. 30, (2013), pp. 13393-13398.
4. R.F.B.D. Souza, A.E.A. Flausino, D.C. Rascio, R.T.E. Oliveira, E.T. Neto, M.L. Calegaro, M.C. Santos, Appl. Catal. B: Environ., Vol. 91, (2009), pp. 516-523.
5. J.W. Guo, T.S. Zhao, J. Prabhuram, R. Chen, C.W. Wong, J. Power Sources, Vol. 156, (2006), pp. 345-354.
6. E.S. Steigerwalt, G.A. Deluga, C.M. Lukehart, J. Phys. Chem. B, Vol. 106, (2002), pp. 760-766.
7. O.S. Alexeev, B.C. Gates, Ind. Eng. Chem. Res., Vol. 42, (2003), pp. 1571-1587.
8. R.J. Gorte, AIChE J., Vol. 56, (2010), pp. 1126-1135.
9. R. Si, Y.W. Zhang, S.J. Li, B.X. Lin, C.H. Yan, J. Phys. Chem. B, Vol. 108, (2004), pp. 12481-12488.
10. M. Kang, M.W. Song, C.H. Lee, Appl. Catal. A, Vol. 251, (2003), pp. 143-156.
11. X. Tang, B. Zhang, Y. Li, Y. Xu, Q. Xin, W. Shen, Catal. Today, Vol. 93, (2004), pp. 191-198.
12. Ch. Xu, R. Zeng, P.K. Shen, Z. Wei, Electrochim. Acta, Vol. 51, (2005), pp. 1031-1035.
13. M.A. Scibioh, S.K. Kim, E.A. Cho, T.H. Lim, S.A. Hong, H.Y. Ha, Appl. Catal. B: Environ, Vol. 84, (2008), pp. 773-82.
14. B.Y. Sarada, K.S. Dhathathreyan, M.R. Krishna, Int. J. hydrogen energy, Vol. 36, (2011), pp. 11886-11894.
15. A.M. Rashidi, M.M. Akbarnejad, A.A. Khodadadi, Y. Mortazavi, EP1782884 A1.
16. Z. Cui, C. Liu, J. Liao, W. Xing, Electrochim. Acta, Vol. 53, (2008), pp. 7807-7811.
17. N.Y. Hsu, C.C. Chien, K.T. Jeng, Appl. Catal. B: Environ, Vol. 84, (2008), pp. 196-203.
18. G. An, P. Yu, L. Mao, Z. Sun, Z. Liu, S. Miao, K. Ding, Carbon, Vol. 45, (2007), pp. 536-542.
19. K.T. Jeng, C.C. Chien, N.Y. Hsu, S.C. Yen, S.D. Chiou, S.H. Lin, W.M. Huang, J. Power Sources, Vol. 160, (2006), pp. 97-104.
20. L.C. Ordonez, P. Roquero, P.J. Sebastian, J. Ramirez, Catal. Today, Vol. 107, (2005), pp. 46-52.
21. T. Frelink, W. Visscher, J.A.R. Vanveen, Electrochim. Acta, Vol. 40, (1995), pp. 545-549.
22. Y.C. Xing, J. Phys. Chem. B, Vol. 108, (2004), pp. 19255-19259.
23. C.W. Xu, P.K. Shen, J. Power Sources, Vol. 142, (2005), pp. 27-29.
24. P. Justin, G.R. Rao, Catal. Today, Vol. 141, (2009), pp. 138-143.
25. J. Qiao, K. Sun, N. Zhang, B. Sun, J. Kong, D. Zhou, J. Power Sources, Vol. 169, (2007), pp. 253-258.
26. X. Yu, S. Ye, J. Power Sources, Vol. 172, (2007), pp. 133-144.
27. P.W. Albers, W. Weber, K. Kunzmann, M. Lopez, S.F. Parker, Surf. Sci., Vol. 602, (2008), pp. 3611-3616.
28. W.J. Zhou, W.Z. Li, S.Q. Song, Z.H. Zhou, L.H. Jiang, G.Q. Sun, Q. Xin, K. Poulianitis, S. Kontoub, P. Tsiakaras, J. Power Sources, Vol. 131, (2004), pp. 217-223.
29. E. Mamontov, W. Dmowski, T. Egami, C.C. Kao, J. Phys. Chem. Solids., Vol. 61, (2000), pp. 431-433.